# A combined use of intravoxel incoherent motion MRI parameters can differentiate early stage hepatitis-b fibrotic livers from healthy livers

Yì Xiáng J. Wáng[1#*], Min Deng[1], Yáo T Li[1], Hua Huang[2], Jason CS Leung[3], Weitian Chen[1], Pu-Xuan Lu[4#]

1 Department of Imaging and Interventional Radiology, Faculty of Medicine, The Chinese University of Hong Kong, Prince of Wales Hospital, New Territories, Hong Kong SAR

2. Department of Radiology, The Shenzhen No. 3 People's Hospital, Shenzhen, Guangdong Province, China.

3. School of Public Health and Primary Care, The Chinese University of Hong Kong, Prince of Wales Hospital, New Territories, Hong Kong SAR

4. Shenzhen Center for Chronic Disease Control, Shenzhen, Guangdong Province, China.

# These two authors contributed equally to this work.

Acknowledgement. The authors thank Dr Jing Yuan, Medical Physics and Research Department, Hong Kong Sanatorium and Hospital, for setting up the data acquisition at the Shenzhen No. 3 People's Hospital.

*Correspondence to: Dr. Yì Xiáng Wáng. Room LG-14, Cancer Center LG-14, Prince of Wales Hospital, Shatin, Hong Kong. Email: yixiang_wang@cuhk.edu.hk

# A combined use of intravoxel incoherent motion MRI parameters can differentiate early stage hepatitis-b fibrotic livers from healthy livers


## Abstract

This study investigated a combined use of IVIM parameters Dslow, PF and Dfast for live fibrosis evaluation. 16 healthy volunteers and 33 hepatitis-b patients (stage F1= 15, stage F2-4 =18) were included. With a 1.5-T MR scanner and respiration-trigger, the IVIM diffusion weighted imaging was acquired with a single-shot echo-planar imaging sequence with ten b-values of 10, 20, 40, 60, 80, 100, 150, 200, 400, and 800 sec/mm$^2$. Signal measurement was performed on right liver. With a 3-D tool, Dslow, PF, and Dfast were placed along the x-axis, y-axis, and z-axis, and a plane was defined to separate healthy volunteers from patients. It was also close to able to differentiate healthy volunteers and all patients with liver fibrosis (F1-4), while healthy volunteers and patients with significant liver fibrosis (F2-4) could be reliably differentiated. Classification and Regression Tree shows a combination of PF (PF<12.55%), Dslow (Dslow<1.152 $\times 10^{-3}$ mm$^2$/s) and Dfast (Dfast<13.36 $\times 10^{-3}$ mm$^2$/s) can differentiate healthy subjects and all fibrotic livers (F1-F4) with an area under the curve of logistic regression (AUC) of 0.986. The AUC for differentiation of F0 vs. F2-4 was 1. PF offers best diagnostic value, followed by Dslow, however all three parameters contribute to liver fibrosis detection.


Keywords: Magnetic resonance imaging (MRI); intravoxel incoherent motion (IVIM); diffusion; perfusion; liver; fibrosis.

Chronic liver disease is a major public health problem worldwide. The epidemic trend of chronic liver disease is expected to increase owing to an aging population, the growing epidemic of obesity and non-alcoholic steatohepatitis. Viral hepatitis is the most common blood-borne infection worldwide [1,2]. Chronic viral hepatitis can lead to hepatic fibrosis, cirrhosis and hepatocellular carcinoma [3]. Liver fibrosis, a common feature of almost all chronic liver diseases, involves the accumulation of collagen, proteoglycans, and other macromolecules in the extracellular matrix [4]. Clinically liver fibrosis usually has an insidious onset and progresses slowly over decades. Originally considered to be irreversible, hepatic fibrosis is now regarded as a dynamic process with the potential for regression [4]. Treatment with combined therapies on underline etiology and fibrosis simultaneously might expedite the regression of liver fibrosis and promote liver regeneration [5-7]. Earlier stage liver fibrosis is more amenable to therapeutic intervention. Even when the underline etiology of liver fibrosis could not be eradicated, therapies on liver fibrosis might help delay the progression of the disease to cirrhosis.

To date, noninvasive diagnostic tests available from clinical practice are not sensitive or specific enough to detect occult liver injury at early stage [8]. Liver biopsy is currently the standard of reference for the diagnosis and staging of liver fibrosis. However, liver biopsy is an invasive procedure with several contraindications and with a risk of complications such as pain, hemorrhage, bile peritonitis, penetration of abdominal viscera, pneumothorax and even death [9,10]. The mortality rate associated with needle biopsy was estimated to be between 0.009% and 0.12% [10]. A noninvasive and quantitative technique for detecting liver fibrosis is highly desirable.

In diffusion-weighted (DW) MRI, the intensity of the acquired magnetic resonance signal depends on the self-diffusion of the excited spins, i.e., on the microscopic stochastic Brownian molecular motion, and the extent and orientation of molecular motion is influenced by the microscopic structure and organization of biological tissues [11-14]. Perfusion can contribute to the diffusion measurements significantly because of the incoherent motion of blood in pseudorandom capillary network at the macroscopic level [15-18]. Intravoxel incoherent motion (IVIM) reflects the random microscopic motion that occurs in voxels on MR images of water molecules (either intra-cellular or extracellular) and the microcirculation of blood. In 1986, Le Bihan *et al* (15,16)

proposed the principle of IVIM which enables the quantitative parameters that separately reflect tissue diffusivity and tissue microcapillary perfusion to be estimated. IVIM signal attenuation is modeled according to the equation

$$SI(b)=SI_0[(1-PF)\cdot\exp^{(-b\cdot Dslow)} + f\cdot\exp^{(-b\cdot Dfast)}], \quad [1]$$

where SI(b) and SI0 denote the signal intensity acquired with the *b*-factor value of *b* and *b*=0 s/mm$^2$, respectively. Perfusion fraction (PF, *f*) is the fraction of the pseudo-diffusion linked to microcirculation, Dslow (or *D*) is the true diffusion coefficient representing the pure molecular diffusion (slow component of diffusion), and Dfast (*D**) is the pseudo-diffusion coefficient representing the incoherent microcirculation within the voxel (perfusion-related diffusion, or fast component of diffusion).

Molecular water diffusion in fibrotic liver would be restricted by the presence of collagen fibers in the distorted lobular structure. Given the relatively high blood volume fraction of <25–30 mL of blood per 100g in liver [19], perfusion can contribute to the diffusion measurements significantly because of the incoherent motion of blood in pseudorandom capillary network at the macroscopic level. It is well accepted that liver fibrosis is associated with reduced liver perfusion [20–23]. Recently there has been greater interest of using IVIM technique to study diffused liver diseases such as liver fibrosis [24]. However, so far the literatures showed IVIM was unable to detect liver fibrosis. We noticed that the potential optimal combination of three IVIM parameters, i.e. Dslow, PF and Dfast, for the detection of liver fibrosis has not been explored in sufficient details. In this study, we set out to explore whether a combination of Dslow, PF and Dfast can be used to separate fibrotic livers from healthy livers. We re-analyze our previously reported cohort, *the Shenzhen 2012/2103 ivim dataset* [25], using our updated understanding for IVIM technique and liver imaging. Our literature review showed the *Shenzhen 2012/2103 ivim dataset* remained one of the largest dataset ever reported with all the patients had biopsy histopathology grading [Fig 10 of reference 24].

## Material and Methods

The characteristics of *the Shenzhen 2012/2013 dataset* has been previously reported [25]. The MRI data was acquired during the period from Aug 1, 2012 to Aug 15, 2013. Sixteen healthy volunteers (10 males, 7 females, mean age: 36.4-yrs old; range: 21–79 yrs old) and 33 consecutively viral hepatitis-b patients were included. The patient cohort had 15 stage F1 subjects (mean age: 31.8 yrs, 22-53 yrs) and 18 stage F2-4 subjects (mean age: 42 yrs, range: 22-53 yrs). The histology diagnosis for liver fibrosis was based on the consensus of the *2000 Xi'an consensus of the Chinese Society of Infectious Disease and Parasitology and the Chinese Society of Hepatology* [26], and being very similar to METAVIR score [27]. Stage 1 (F1) of liver fibrosis is mild fibrosis only seen at the portal area; stage 2 (F2) indicates fibrosis extending out from the portal areas with rare bridges between portal areas, but without the destruction of the lobular structure; stage 3 (F3) of liver fibrosis is severe fibrosis, there is fibrotic bridging between portal areas and between portal areas and center veins; In stage 4 (F4) there are pseudo-lobules formed and this stage is the final stage of cirrhosis. Hepatic fibrosis (F0, F1) are commonly referred to as no significant hepatic fibrosis; hepatic fibrosis (F2, F3, and F4) are commonly referred to as significant hepatic fibrosis, and F4 is referred as cirrhosis [28]. Hepatic fibrosis could be considered clinically significant if defined as F2 or greater than F2, and deserved medical attention [28, 29]

MR imaging was performed with a 1.5-T magnet (Achieva, Philips Healthcare, Netherlands). The IVIM DW imaging sequence was based on a single-shot DW spin-echo type echo-planar imaging sequence, with ten *b*-values of 10, 20, 40, 60, 80, 100, 150, 200, 400, 800 sec/mm$^2$ respectively. SPIR technique (Spectral Pre-saturation with Inversion-Recovery) was used for fat suppression. The respiratory-gating resulted in an average TR of 1500 msec, and the TE was 63 msec. Other parameters included slice thickness =7 mm, matrix: 124×97, FOV =375 mm×302 mm, NEX=2, number of slices =6. The IVIM signal attenuation was modeled according to the Equation [1]. The estimation of D was obtained by a least-squares linear fitting of the logarithmized image intensity at the *b*-values greater than 200 sec/mm2 to a linear equation. The fitted curve was then extrapolated to obtain an intercept at b=0. The ratio between this intercept and the $SI_0$, gave an estimate of PF. Finally, the obtained Dslow and PF were substituted into Eq. [1] and were non-

linear least-square fitted against all *b*-factors to estimate Dfast using the Levenberg- Marquardt algorithm.

All curve fitting algorithms were implemented in an accustom program develop on MatLab (Mathworks, Natick, MA, USA). Regions-of-interest (ROIs) were positioned to cover a large portion of liver parenchyma while avoiding large vessels (Fig 1). For ROI analysis, the IVIM parameters were calculated based on the mean signal intensity of the whole ROI, which give better estimation than pixel-wise fitting when the signal-to-noise of the DW images is low [30, 31].

The following modifications were made for measurement compared with our previous report [25]. Left lobe of liver is more likely to suffer from artifacts associated the cardiac motion, and susceptibility B0 inhomogeneity due its proximity to the stomach and its air inside, therefore in the current study only the right lobe was measured (Fig 1). Fig 1 demonstrated ROI was carefully drawn to cover only liver parenchyma while avoiding vasculature and artifacts. All 6 slice per subject were evaluated, while the slices with notable motion artifacts and those demonstrates notable outlier with signal *b*-value relation were discarded, and finally the slice used for final analysis varied between two to five slices (average: three slices). In addition, with careful histopathology review, two patients with F1 histology score were re-defined as into F2. The overall results of current analysis did not differ very notably with previous analysis [25].

We applied a 3-dimensional tool programed using IBM SPSS 23 for Windows (SPSS Inc., Chicago, IL, USA), and placed the measures of Dslow, PF, and Dfast placed along the x-axis, y-axis, and z-axis. In this study, data points from healthy volunteer were labeled as blue, F1 patients labeled as pink, and patient labeled as red. Attempts were made visually to separate healthy volunteers from patients (F1-F4); healthy volunteers from significant patients (F2-F4); and separate patients with different stages.

The Support Vector Machine (SVM) approach was used to quantitatively separate the F0 from F1-F4, or F0 from F2-F4 [32]. SVM was used to find a plane (parametrized as Ax+By+Cz+D = 0) that is able to separate the data points into two groups. We define the distance of the closest data point from an individual group to the separating plane as $d_i$, where i represents the index of the group. We use the SVM algorithm to find an optimal plane which maximizes the margin defined as $d_1 + d_2$. Prior to calculate the distance$d_i$, the measured Dslow, PF, and Dfast are normalized by the following equation.

$z(i) = (x(i)-x_{min})/(x_{max}-x_{min})$

where x(i) is the original data and z(i) is the normalized data; $x_{max}$ and$x_{min}$ are the maximum and the minimum value of x(i), respectively. Note the range of z(i) after normalization is from 0 to 1 for each dimension.

Classification and Regression Tree (CART) model was used to find the cut-off values for PF, Dslow, and Dfast to differentiate F0 vs. F1-4 and F0 vs. F2-4 [33].

## Results

Livers of healthy volunteers had PF of 16.6%±3.6% (mean ± standard deviation), Dslow of 1.14±0.22 ($\times 10^{-3}$ $mm^2/s$), and Dfast of 12.3 ±3.1 ($\times 10^{-3}$ $mm^2/s$) respectively. The CoV (coefficient of variation, SD/mean) of PF, Dslow and Dfast in healthy volunteers was 0.19, 0.22, and 0.25, respectively. We grouped the participants into three group, 1) healthy volunteers (F0), 2) insignificant liver fibrosis (F1), and 3) significant liver fibrosis (F2, F3, F4). It was seen that PF offered best differentiation of the three group, followed by Dslow, while Dfast offered little differentiation (Table 1, Figure-2).

By adjusting the viewing angel, the 3-dimensional visual tool demonstrated it was also close to possible to differentiate healthy volunteers (F0, n=16) and all patients with liver fibrosis (F1-4, n=33, Fig 3), while healthy volunteers (F0, n=16) and patients with significant liver fibrosis (F2-4, n=18) could be confidently differentiated (Fig 4). The cluster of F1 subjects was between F0 and

F2-4 (3); however, it was not possible to clearly differentiate patients of different stages (supplementary video-1, 2).

Quantitative analysis with SVM showed healthy volunteers and all patients with liver fibrosis (F1-4) were differentiated with a plane defined by *(166.58*PF) +(8.90*Dslow) - (0.98*Dfast) -19.71=0* (Fig 3); healthy volunteers and patients with significant liver fibrosis (F2-4) were differentiated with a plane defined by *(29.56*PF) + (4.33*Dslow) - (0.12*Dfast)-6.67=0* (Fig 4). The mean distance of the data points for F0 and F2-4 to the central plane was $0.0149_{F0}+0.0138_{F2-4}= 0.0287$, and for F0 vs F1-4 to the central plane was $0.0021_{F0}+0.0026_{F1-2}= 0.0047$.

Three-dimensional visual tool demonstrated better differentiation than 2-dimensional plot using PF and Dslow values, indicating Dfast contributed to differentiate healthy volunteers and patients with liver fibrosis (Fig3-5).

The CART analysis result is shown in table 2, a combination of PF (cutoff value: PF<12.55%), Dslow (Dslow< 1.152 $\times 10^{-3}$ $mm^2/s$) and Dfast (Dfast<13.36 $\times 10^{-3}$ $mm^2/s$) can differentiate healthy subjects (F0) and fibrotic livers (F1-F4) with an AUC (Area under the curve of logistic regression) of 0.986. The AUC for differentiation of F0 vs. F2-4 was 1.

## Discussion

The PF and Dslow measurement obtained in this study broadly agreed with previous reports [25, 30-35]. For the 27 studies which reported measurement for healthy livers, the median value for Dslow was 1.11×10-3 $mm^2/s$ and 1.02×10-3 $mm^2/s$ at 1.5 and 3 T respectively; the median value for PF was 22.00% and 22.65% at 1.5 and 3T respectively. Using a 25 *b*-values acquisition, ter Voert *et al* [34] reported CoV of 0.23, 0.22, 0.68 for PF, Dslow and Dfast for the normal liver regions of 15 subjects. For healthy subjects, the CoV in this study was 0.21, 0.19 and 0.25 for PF, Dslow and Dfast respectively. In five previous studies, CoV for PF and Dslow in healthy subjects have been reported to be 0.13 and 0.11 [35], 0.30 and 0.21 [36], 0.28 and 0.19 [37], 0.20 and 0.64 [38], 0.18 and 0.05 [39]. Therefore, the ivim quantitative measurement of *Shezhen201/2013*

*ivim dataset* are broadly comparable to other reported results. Dfast value obtained in this study is lower than most of the previous reports [24]. The computing of Dfast, and to a less extent also the PF, is expected to have been comprised by that we did not obtain *b*=0 images for the *Shezhen201/2013 ivim dataset* (supplementary document 1). The Dfast is more related to the low *b*-values (<50 s/mm$^2$), which corresponds to the steep part in the measured signal versus b-value relationship, while this relationship is virtually linear in the parts of 100–800 s/mm$^2$ (area most influenced by Dslow, Fig 5 of reference 24).

Though many researches have been published on the evaluation of liver fibrosis using IVIM, how to optimally combine Dslow, PF, and Dfast to get diagnostic information is not yet explored. The most important result of the current study is that despite the *Shezhen201/2013 ivim dataset* was not acquired with optimized protocol, particularly *b*-value distribution, still we were able to demonstrate that healthy volunteers and patients with significant liver fibrosis (F2-4) can be reliably differentiated, and it is also close to feasible to differentiate healthy volunteers and all patients with liver fibrosis (F1-4). Another important finding of this study is that among PF, Dslow and Dfast, PF offers best diagnostic value; and Dfast can provide additional differentiation value despite it is a less stable measurement. It can be seen that overall the cluster of F1 subjects was between F0 and F2-4 (3); however, it is still impossible to clearly differentiate patients of different stages. We expect this is at least partially due to the fact that the histological diagnosis is also not a clear-cut, a high end F1 liver will be similar to a lower end F2 liver [40]. The findings of this study are important as till now it has been considered that there is no reliable noninvasive method, being imaging or serum biomarkers, can detect early stage liver fibrosis. In the meantime, we are looking into further validating our approach with other dataset or with new prospective studies.

IVIM parameters strongly depend upon the choice of the *b*-value and the threshold used for computation. Numerical modeling suggests that the estimation uncertainties of Dslow and PF can reach 3.89% and 11.65% respectively with typical parameter values at a moderate signal-to-noise ratio (SNR) of 40 [41]. However, to estimate Dfast within 10% uncertainty requires SNR>122 [41]. Pekar *et al.* [42] commented that Dfast in particular tends to be unstable unless an

unrealistically high SNR is achieved. Optimization of b-value distribution may improve PF measurement. More *b*-values and applying an optimized b value distribution reduce errors in the IVIM parameter estimation [24, 30, 43-46]. In ter Voert's study, the imaging time for IVIM was 5 to 6 minutes with 25 b-value which is clinically acceptable. Empirical literatures also suggest that Dslow is the most reliable parameter among the three parameters [24]. However, Dslow may suffer from limited dynamic range for detecting fibrotic changes in the liver as shown this study. On the other hand, PF may offer both reasonable measurement stability and sufficient dynamic range.

There are a few ways to improve the measurement accuracy in this study. The right cut-off *b*-value to compute PF needs further investigation, as this will impact the measurement of all three parameters. According to recent analysis [24], the cut-off *b*-value to obtain Dslow for this study, i.e. *b*=200, may be too high. It will be worthwhile test to assign only *b*-value of less than 50 as low *b*-value. Diffusion weighted imaging is very sensitive to any macroscopic patient motions. The most important sources of such motion are respiratory motion, pulsatile blood flow and cardiac motion. In the presence of B0 inhomogeneities and susceptibility variations, single-shot spin-echo echo-planar imaging sequence frequently suffer from gross geometrical image distortions. Susceptibility variations translate to variations of the Larmor frequencies of spins and, thus, to phase errors in the k-space data that accumulate over the duration of the echo train [14]. A second disadvantage of single-shot echo planar imaging is the relatively low spatial resolution. Parallel imaging can be used to reduce the echo-train length and, thus, the geometric distortions in echo-planar imaging and, or to increase the spatial resolution. Finally, due to the extensive respiratory motion during free breathing or residual motion from respiratory gated data acquisition, it may be beneficial to use breath-hold technique [24]. Our previous experience suggests that it is possible to get precise liver tissue measurement even by multiple breath-hold [47]. Another point is to de-noise as well as design better segmentation approach to statistically remove ill-fitted pixels in ROI, and employing better fitting strategies [48-52].

Another limitation of our study is all our patients had liver fibrosis due to viral hepatitis-b. Whether results of our study can be generalized to liver fibrosis of other causes, most commonly

NASH, remains to be validated. It is expected that with better IVIM imaging protocol with more *b*-values and better image post-procession, differentiation of early stage fibrotic liver from healthy liver should have increased reliability. Another point is that quantification diffusion coefficient may be confounded by fat and iron in the liver [53], and this has not been carefully investigated in this study. However, it has been shown that imaging can reliably detect late stage liver fibrosis and liver cirrhosis [54]. The question which requires important attention is to detect F1 and F2 stage liver fibrosis. Additionally, liver fat and iron can reliably be quantified by MRI [55, 56]. The use of Bayesian prediction, incorporating relevant findings from the available methods, is also a promising technique for liver fibrosis evaluation [57]. The Bayesian prediction provides probabilities, rather than a 'yes/no' decision. The Bayesian method also allows weighting of the different methods, such as IVIM, liver T1rho, and elastography readouts [58-56], therefore realizing multi-parameter diagnosis.

In conclusion, a combination of PF, Dslow and Dfast shows the potential of IVIM to detect early stage liver fibrosis. Among the three parameters PF offer best diagnostic value, followed by Dslow, however, all three parameters contribute to liver fibrosis evaluation. Further researches shall include improving image data post-processing and denoise poorly fitted regions in the liver, and also validating our approach with additional datasets.

Footnote: *The Shenzhen 2012/2103 ivim dataset* are available to external researchers for additional analysis upon contacting the corresponding author of this article.

## References

1. Wanich N, Vilaichone RK, Chotivitayatarakorn P, Siramolpiwat S. High Prevalence of Hepatocellular Carcinoma in Patients with Chronic Hepatitis B Infection in Thailand. *Asian Pac J Cancer Prev.* 2016;17:2857-60.

2. Chak E, Talal AH, Sherman KE, Schiff ER, Saab S. Hepatitis C virus infection in USA: an estimate of true prevalence. *Liver Int.* 2011;31(8):1090-101.

3. Weiskirchen R, Tacke F. Liver Fibrosis: From Pathogenesis to Novel Therapies. *Dig Dis.* 2016;34(4):410-22.

4. Wallace K, Burt AD, Wright MC. Liver fibrosis. *Biochem J* 2008; 411: 1–18.

5 . Friedman SL. Hepatic fibrosis: overview. *Toxicology* 2008; 254:120–129

6. Sanyal AJ, Friedman SL, McCullough AJ, Dimick-Santos L; American Association for the Study of Liver Diseases; United States Food and Drug Administration. Challenges and opportunities in drug and biomarker development for nonalcoholic steatohepatitis: findings and recommendations from an American Association for the Study of Liver Diseases-U.S. Food and Drug Administration Joint Workshop. *Hepatology* 2015;61:1392-405.

7. Wang P, Koyama Y, Liu X, Xu J, Ma HY, Liang S, Kim IH, Brenner DA, Kisseleva T. Promising Therapy Candidates for Liver Fibrosis. *Front Physiol* 2016;7:47.

8. Patel K, Shackel NA. Current status of fibrosis markers. *Curr Opin Gastroenterol* 2014; 30: 253–

9. Bravo AA, Sheth SG, Chopra S. Liver biopsy. *N Engl J Med* 2001;344: 495–500

10. Tobkes AI, Nord HJ. Liver biopsy: review of methodology and complications. *Gig. Dis*. 1995; 13: 267–274.

11. Hahn EL. Spin echoes. *Phys Rev* 1950;80(4):580–94.

12. Stejskal EO, Tanner JE. Spin diffusion measurements: spin echoes in the presence of a time-dependent field gradient. *J Chem Phys* 1965;42(1):288–9

13. Winston GP. The physical and biological basis of quantitative parameters derived from diffusion MRI. *Quant Imaging Med Surg.* 2012;2(4):254-65.

14. Dietrich O, Biffar A, Baur-Melnyk A, Reiser MF. Technical aspects of MR diffusion imaging of the body. *Eur J Radiol.* 2010;76(3):314-22.

15. Le Bihan D, Breton E, Lallemand D, Grenier P, Cabanis E, Laval-Jeantet M. MR imaging of intravoxel incoherent motions: application to diffusion and perfusion in neurologic disorders. *Radiology* 1986;161:401-7.

16. Le Bihan D, Breton E, Lallemand D, Aubin ML, Vignaud J, Laval-Jeantet M. Separation of diffusion and perfusion in intravoxel incoherent motion MR imaging. *Radiology* 1988;168:497-505.

17. Le Bihan D, Turner R. The capillary network: a link between IVIM and classical perfusion. *Magn Reson Med* 1992;27:171-8.

18 . Le Bihan D, Turner R, Moonen CT, Pekar J. Imaging of diffusion and microcirculation with gradient sensitization: design, strategy, and significance. *J Magn Reson Imaging* 1991;1:7-28.

19. Greenway CV, Stark RD. Hepatic vascular bed. *Physiol Rev* 1971;51:23-65.

20. Moreno AH, Burchell AR, Rousselot LM, Panke WF, Slafsky F, Burke JH. Portal blood flow in cirrhosis of the liver. *J Clin Invest* 1967; 46: 436–445.

21. Iwakiri Y, Groszmann RJ. The hyperdynamic circulation of chronic liver diseases: from the patient to the molecule. *Hepatology* 2006;43(2 Suppl 1):S121-31.

22. Van Beers BE, Leconte I, Materne R, Smith AM, Jamart J, Horsmans Y. Hepatic perfusion parameters in chronic liver disease: dynamic CT measurements correlated with disease severity. *Am J Roentgenol* 2001; 176: 667–673.

23. Blendis L, Wong F. The hyperdynamic circulation in cirrhosis: an overview. *Pharmacol Ther.* 2001;89(3):221-31.

24. Li YT, Cercueil JP, Yuan J, Chen W, Loffroy R, Wáng YX. Liver intravoxel incoherent motion (IVIM) magnetic resonance imaging: a comprehensive review of published data on normal values and applications for fibrosis and tumor evaluation. *Quant Imaging Med Surg.* 2017;7(1):59-78.

25. Lu PX, Huang H, Yuan J, Zhao F, Chen ZY, Zhang Q, Ahuja AT, Zhou BP, Wáng YX. Decreases in molecular diffusion, perfusion fraction and perfusion-related diffusion in fibrotic livers: a

prospective clinical intravoxel incoherent motion MR imaging study. *PLoS One.* 2014;9(12):e113846.

26. The Chinese Society of Infectious Disease and Parasitology and the Chinese Society of Hepatology. [Guidelines for prevention and treatment of viral hepatitis] (in Chinese). *Chin J Infect Dis* 2001; 19 (1): 56-62

27. Bedossa P, Poynard T The METAVIR Cooperative Study Group. (1996) An algorithm for the grading of activity in chronic hepatitis C. *Hepatology* 1996 24: 289–293.

28. Pavlov CS, Casazza G, Nikolova D, Tsochatzis E, Burroughs AK, Ivashkin VT, Gluud C. Transient elastography for diagnosis of stages of hepatic fibrosis and cirrhosis in people with alcoholic liver disease. *Cochrane Database Syst Rev.* 2015 Jan 22;1:CD010542.

29. Franciscus A. HCV diagnostic tools: grading and staging a liver biopsy (version 2.2). www.hcvadvocate.org

30. Yuan J, Wong OL, Lo GG, Chan HH, Wong TT, Cheung PS. Statistical assessment of bi-exponential diffusion weighted imaging signal characteristics induced by intravoxel incoherent motion in malignant breast tumors. *Quant Imaging Med Surg.* 2016;6(4):418-429.

31. Li YT, Huang H, Zhuo Z, Lu PX, Chen W, Wáng YX. Bi-phase age-related brain gray matter magnetic resonance T1ρrelaxation time change in adults. *Mag Reson Imaging* 2017

32. Chang CC, Lin C-J. LIBSVM: a library for support vector machines. ACM Transactions on Intelligent Systems and Technology (TIST) 2011;2:27.

33. Woo J, Leung J. Anthropometric Cut Points for Definition of Sarcopenia Based on Incident Mobility and Physical Limitation in Older Chinese People. *J Gerontol A Biol Sci Med Sci.* 2016;71(7):935-40.

34. ter Voert EE, Delso G, Porto M, Huellner M, Veit-Haibach P. Intravoxel Incoherent Motion Protocol Evaluation and Data Quality in Normal and Malignant Liver Tissue and Comparison to the Literature. *Invest Radiol* 2016;51:90-9.

35. Chung SR, Lee SS, Kim N, Yu ES, Kim E, Kühn B, Kim IS. Intravoxel incoherent motion MRI for liver fibrosis assessment: a pilot study. *Acta Radiol* 2015;56:1428-36.

36, Ichikawa S, Motosugi U, Morisaka H, Sano K, Ichikawa T, Enomoto N, Matsuda M, Fujii H, Onishi H. MRI-based staging of hepatic fibrosis: Comparison of intravoxel incoherent motion diffusion-weighted imaging with magnetic resonance elastography. *J Magn Reson Imaging* 2015;42:204-10.

37. Wu CH, Ho MC, Jeng YM, Liang PC, Hu RH, Lai HS, Shih TT. Assessing hepatic fibrosis: comparing the intravoxel incoherent motion in MRI with acoustic radiation force impulse imaging in US. *Eur Radiol* 2015;25:3552-9.

38. Luciani A, Vignaud A, Cavet M, Nhieu JT, Mallat A, Ruel L, Laurent A, Deux JF, Brugieres P, Rahmouni A. Liver cirrhosis: intravoxel incoherent motion MR imaging--pilot study. *Radiology* 2008;249:891-9

39. Hayashi T, Miyati T, Takahashi J, Fukuzawa K, Sakai H, Tano M, Saitoh S. Diffusion analysis with triexponential function in liver cirrhosis. *J Magn Reson Imaging* 2013;38:148-53.

40. Bedossa P, Dargere D, Paradis V. Sampling variability of liver fibrosis in chronic hepatitis C. *Hepatology* 2003; 38:1449–1457

41. Zhang Q, Wang YX, Ma HT, Yuan J. Cramér-Rao bound for Intravoxel Incoherent Motion Diffusion Weighted Imaging fitting. *Conf Proc IEEE Eng Med Biol Soc.* 2013;2013:511-4.

42. Pekar J, Moonen CT, van Zijl PC. On the precision of diffusion/perfusion imaging by gradient sensitization. *Magn Reson Med* 1992;23:122-9.

43. Lemke A, Stieltjes B, Schad LR, Laun FB. Toward an optimal distribution of b values for intravoxel incoherent motion imaging. *Magn Reson Imaging* 2011;29:766-76.

44. Gurney-Champion OJ, Froeling M, Klaassen R, Runge JH, Bel A, van Laarhoven HW, Stoker J, Nederveen AJ. Minimizing the Acquisition Time for Intravoxel Incoherent Motion Magnetic Resonance Imaging Acquisitions in the Liver and Pancreas. *Invest Radiol* 2016;51:211-20.

44. Wurnig MC, Donati OF, Ulbrich E, Filli L, Kenkel D, Thoeny HC, Boss A. Systematic analysis of the intravoxel incoherent motion threshold separating perfusion and diffusion effects: Proposal of a standardized algorithm. *Magn Reson Med* 2015;74:1414-22.

46. Lemke A, Laun FB, Simon D, Stieltjes B, Schad LR. An in vivo verification of the intravoxel incoherent motion effect in diffusion-weighted imaging of the abdomen. *Magn Reson Med* 2010;64:1580-5.

47. Deng M, Zhao F, Yuan J, Ahuja AT, Wang YX. Liver T1ρ MRI measurement in healthy human subjects at 3 T: a preliminary study with a two-dimensional fast-field echo sequence. *Br J Radiol.* 2012;85(1017):e590-5.

48. Yuan J, Wong OL, Lo GG, Chan HH, Wong TT, Cheung PS. Statistical assessment of bi-exponential diffusion weighted imaging signal characteristics induced by intravoxel incoherent motion in malignant breast tumors. *Quant Imaging Med Surg*. 2016;6(4):418-429.

49. Freiman M, Perez-Rossello JM, Callahan MJ, Voss SD, Ecklund K, Mulkern RV, Warfield SK. Reliable estimation of incoherent motion parametric maps from diffusion-weighted MRI using fusion bootstrap moves. *Med Image Anal* 2013;17:325-36.

50. Zhang Q, King AD, Bhatia KS, Yeung DK, Wang YX, Liang D, Yuan J. Improving intra-voxel incoherent motion MRI quantification using wild bootstrap. 2014 *IEEE 11th International Symposium on Biomedical Imaging (ISBI)* 2014:726-9.

51. Wang Z. Improving cerebral blood flow quantification for arterial spin labeled perfusion MRI by removing residual motion artifacts and global signal fluctuations. *Magn Reson Imaging* 2012;30(10):1409-15.

52. Neil JJ, Bretthorst GL. On the use of Bayesian probability theory for analysis of exponential decay data: an example taken from intravoxel incoherent motion experiments. *Magn Reson Med* 1993;29:642-7

53. Bülow R, Mensel B, Meffert P, Hernando D, Evert M, Kühn JP. Diffusion-weighted magnetic resonance imaging for staging liver fibrosis is less reliable in the presence of fat and iron. *Eur Radiol.* 2013;23(5):1281-7.

54. Faria SC, Ganesan K, Mwangi I, Shiehmorteza M, Viamonte B, Mazhar S, Peterson M, Kono Y, Santillan C, Casola G, Sirlin CB. MR imaging of liver fibrosis: current state of the art. *Radiographics.* 2009;29(6):1615-35.

55. Wunderlich AP, Cario H, Juchems MS et al. Noninvasive MRI-Based Liver Iron Quantification: Methodic Approaches, Practical Applicability and Significance. *Fortschr Röntgenstr* 2016; 188: 1031 - 1036.

56. Di Martino M, Pacifico L, Bezzi M, Di Miscio R, Sacconi B, Chiesa C, Catalano C. Comparison of magnetic resonance spectroscopy, proton density fat fraction and histological analysis in the quantification of liver steatosis in children and adolescents. *World J Gastroenterol.* 2016;22(39):8812-8819.

57. Motosugi U, Ichikawa T, Araki T, Matsuda M, Fujii H, Enomoto N. Bayesian prediction for liver fibrosis staging: combined use of elastography and serum fibrosis markers. *Hepatology* 2013;58(1):450-1.

58. Wang YX, Yuan J. Evaluation of liver fibrosis with T1ρ MR imaging. *Quant Imaging Med Surg.* 2014;4(3):152-5.

59. Koon CM, Zhang X, Chen W, Chu ES, San Lau CB, Wáng YX. Black blood T1rho MR imaging may diagnose early stage liver fibrosis: a proof-of-principle study with rat biliary duct ligation model. *Quant Imaging Med Surg.* 2016;6(4):353-363.

60. Leung VY, Shen J, Wong VW, Abrigo J, Wong GL, Chim AM, Chu SH, Chan AW, Choi PC, Ahuja AT, Chan HL, Chu WC. Quantitative elastography of liver fibrosis and spleen stiffness in chronic hepatitis B carriers: comparison of shear-wave elastography and transient elastography with liver biopsy correlation. *Radiology*. 2013;269(3):910-8.

61. Chang W, Lee JM, Yoon JH, Han JK, Choi BI, Yoon JH, Lee KB, Lee KW, Yi NJ, Suh KS. Liver Fibrosis Staging with MR Elastography: Comparison of Diagnostic Performance between Patients with Chronic Hepatitis B and Those with Other Etiologic Causes. *Radiology.* 2016;280(1):88-97.

Table 1, Mean, standard deviation (sd), and (CoV) of PF, Dslow, and Dfast of healthy volunteers, F1 liver fibrosis patients, and F2-4 liver fibrosis patients.

| | PF | | | Dslow $\times 10^{-3}$ mm$^2$/s | | | Dfast $\times 10^{-3}$ mm$^2$/s | | |
|---|---|---|---|---|---|---|---|---|---|
| | F0 | F1 | F2-4 | F0 | F1 | F2-4 | F0 | F1 | F2-4 |
| mean | 0.165 | 0.11 | 0.091 | 1.14 | 1.01 | 0.94 | 12.34 | 12.03 | 11.68 |
| sd | 0.036 | 0.017 | 0.019 | 0.22 | 0.14 | 0.13 | 3.06 | 1.85 | 2.22 |
| CoV | 0.215 | 0.157 | 0.211 | 0.19 | 0.14 | 0.14 | 0.25 | 0.15 | 0.19 |

Table 2. CART analysis of area under the curve of logistic regression (AUC) of F1-4 or F2-4 (comparing with F0) on PF, Dslow and Dfast

| Model | AUC (1): F1-4 vs F0 | AUC (2): F2-4 vs F0 |
|---|---|---|
| PF | 0.9545 (cutoff value: *PF<0.1255*) | 1 (cutoff value: *PF<0.123*) |
| PF and Dslow | 0.9773 (cutoff value: *Dslow< 1.152*) | 1 (cutoff value: *Dslow< 1.131*) |
| PF, Dslow and Dfast | 0.9858 (cutoff value: *Dfast<13.36*) | 1 (cutoff value: *Dfast<13.3*) |

Unit of Dslow and Dfast: $\times 10^{-3}$ mm$^2$/s

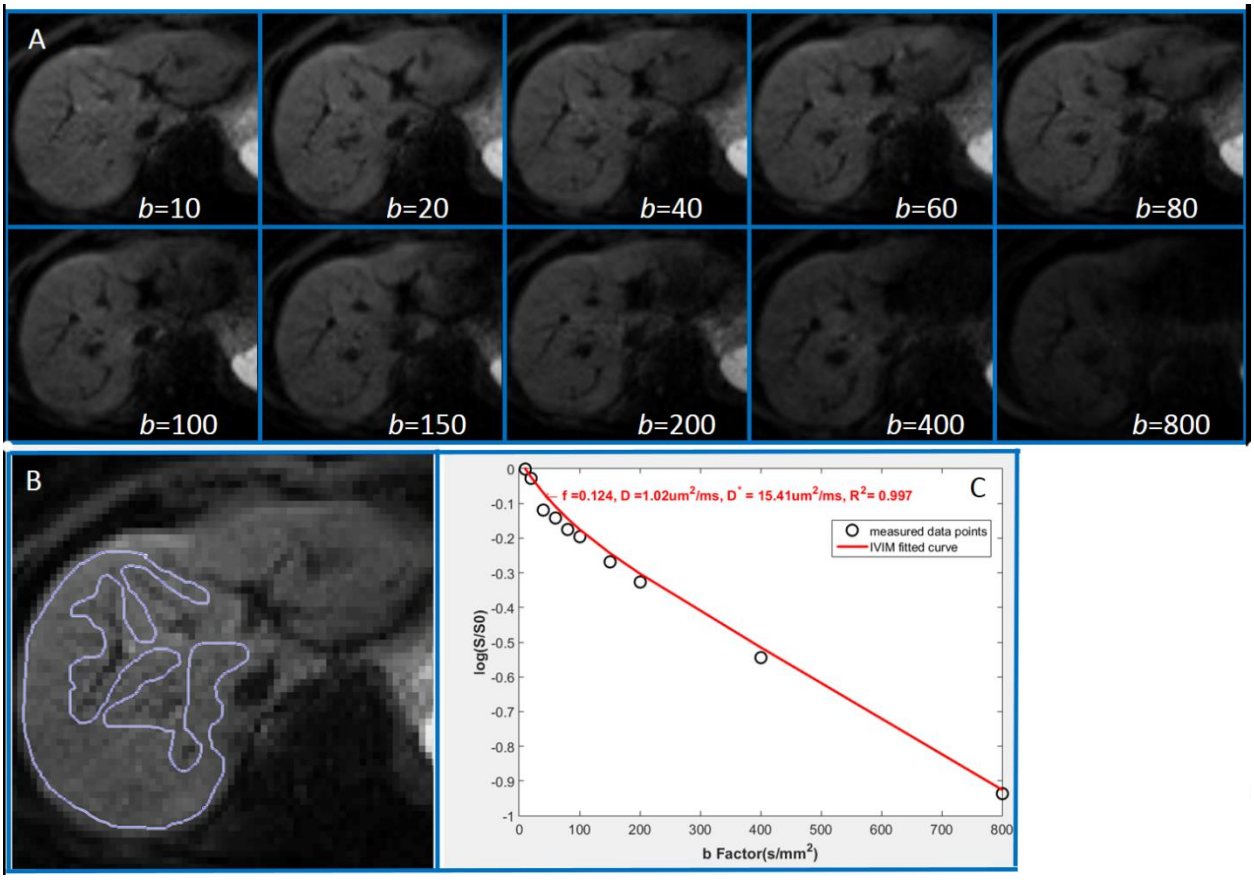


Fig 1. A: Demonstration of a diffusion weighted images with ten *b*-values from a participant; B: Demonstration of a careful ROI drawing to avoid liver vasculature; C: Signal and *b*-value relationship of the liver slice in B.

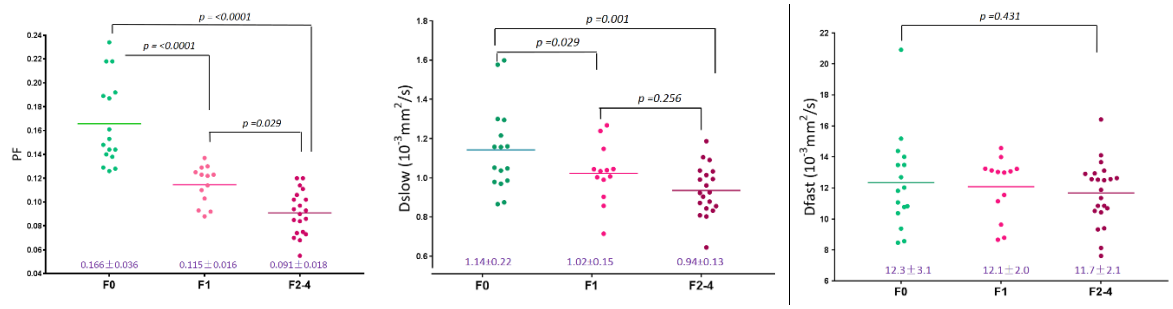


Fig 2, Scattered plots and mean of PF, Dslow, and Dfast of healthy volunteers, F1 liver fibrosis patients, and F2-4 liver fibrosis patients (*p*-value: ANOVA and Mann Whitney U test)

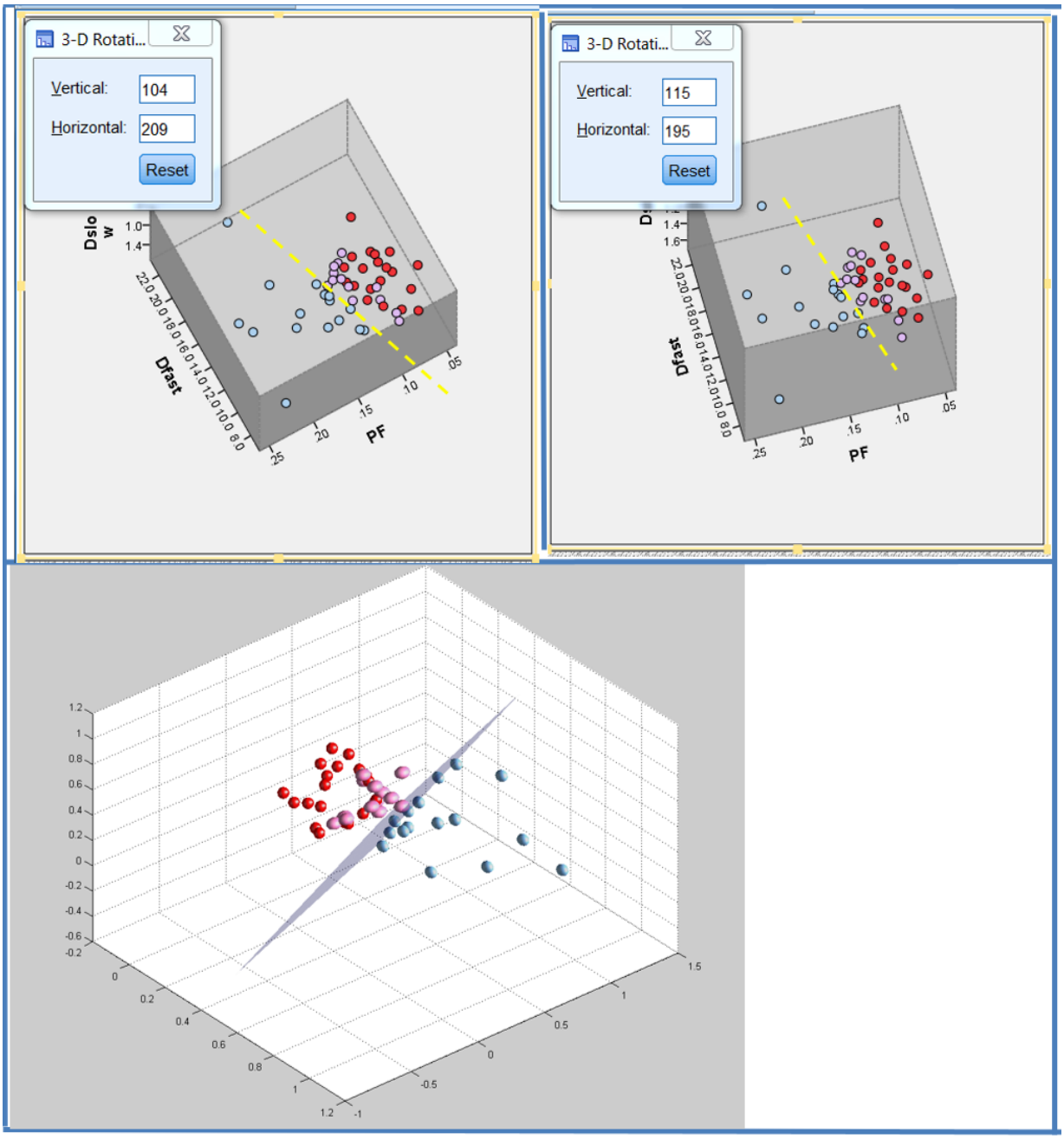


Fig 3, three-dimensional display of healthy volunteer group (blue balls), F1 patient group (pink balls), and F2-3 patient group (red balls). Each ball represents one participant. The differentiation (dotted yellow line) of volunteer group and patient group can be better visualized by rotating in 3-D space.

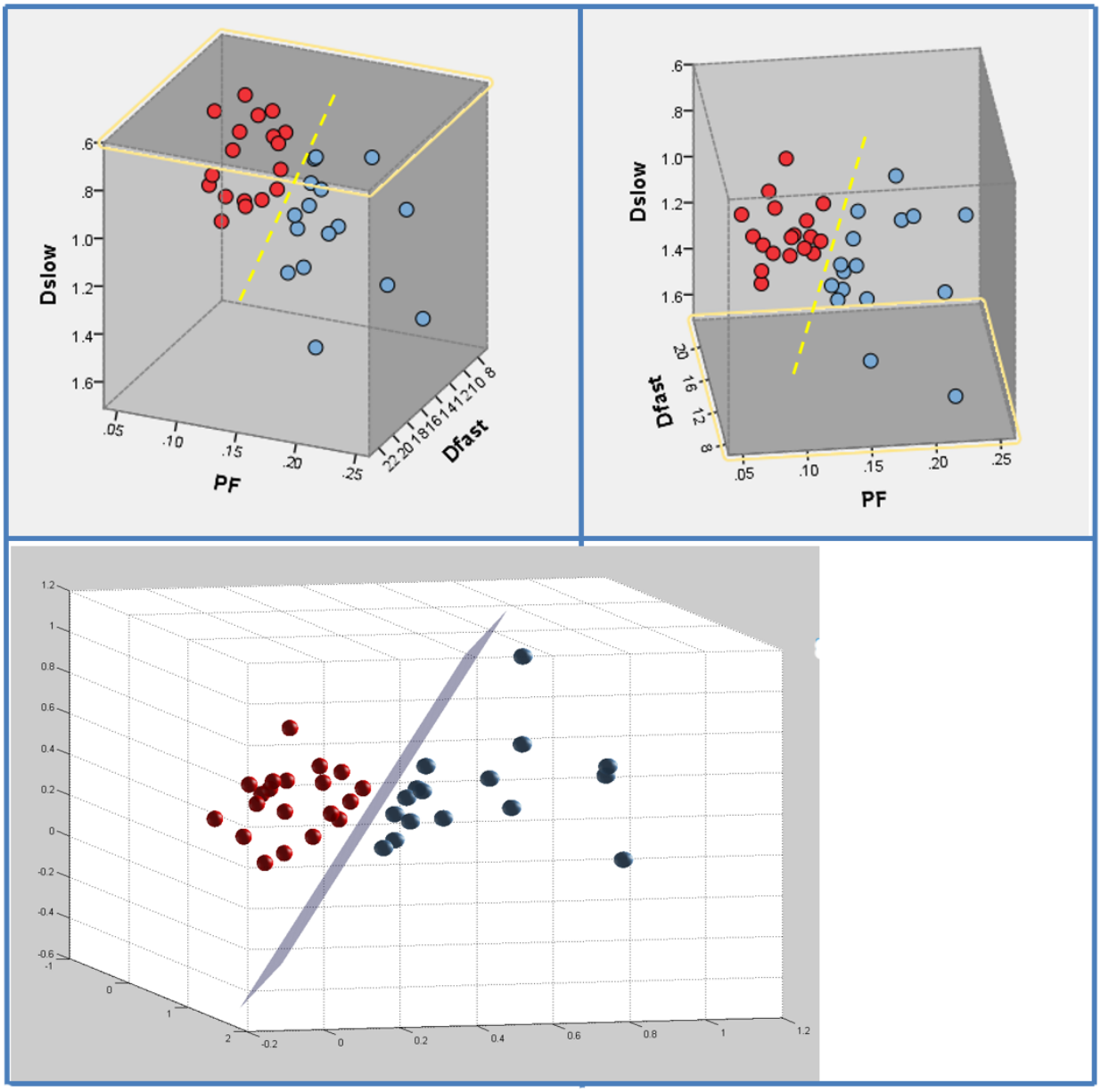


Fig 4, three-dimensional display of healthy volunteer group (blue balls), and F2-3 patient group (red balls). Each ball represents one participant. The differentiation (dotted yellow line) of volunteer group and patient group (F1-4) can be better visualized by rotating in 3-D space.

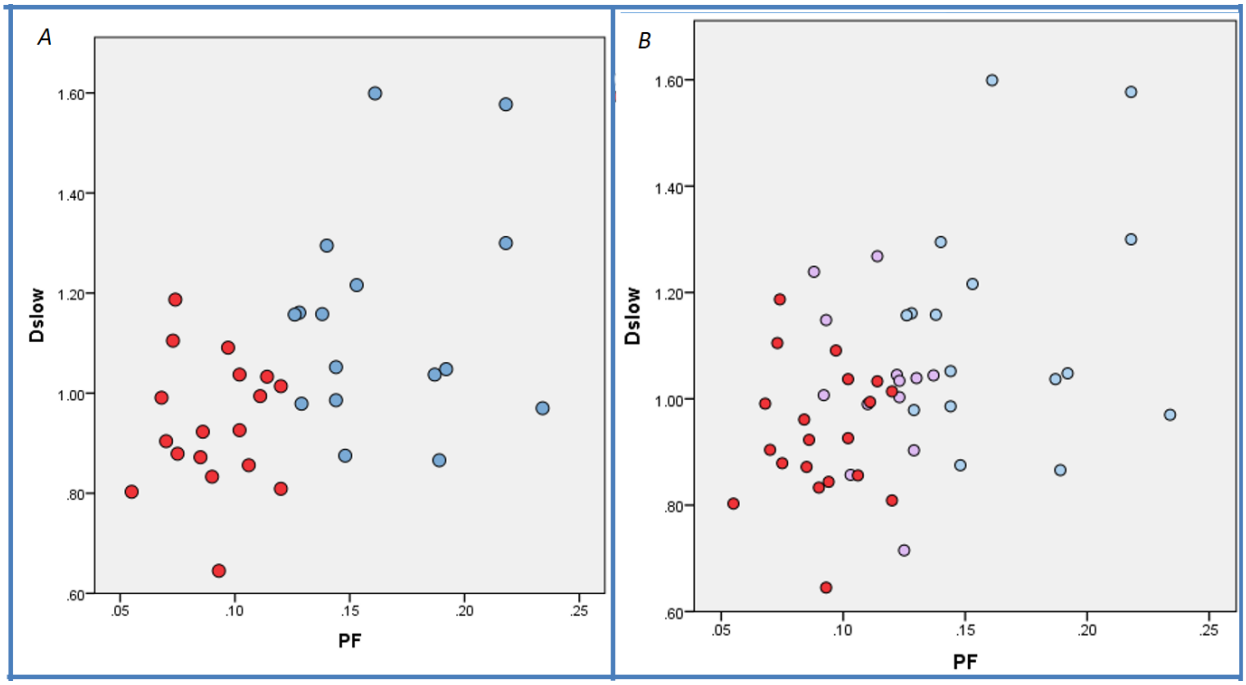


Fig 5, two-dimensional demonstration of healthy volunteer group (blue balls), and F1 patient group (pink balls), and F2-3 patient group (red balls) using PF-axis and Dslow-axis. Each ball represents one participant. A combination of PF-axis and Dslow-axis is insufficient to differentiate F0 subjects and F1-4 patients, in contrast to demonstrations in Fig 3 and Fig 4.